Japanese Journal of Radiology
https://doi.org/10.1007/s11604-020-00966-w

ORIGINAL ARTICLE

Performance evaluation of developed dedicated breast PET scanner and improvement of the spatial resolution by wobbling: a Monte Carlo study

Azadeh Emami[1,2,3] · Hossein Ghadiri[1,2] · Pardis Ghafarian[4,5] · Parham Geramifar[6] · Mohammad Reza Ay[1,2]

Received: 15 November 2019 / Accepted: 26 March 2020

Abstract

Purpose Molecular imaging, particularly PET scanning, has become an important cancer diagnostic tool. Whole-body PET is not effective for local staging of cancer because of their declining efficiency in detecting small lesions. The preliminary results of the performance evaluation of designed dedicated breast PET scanner presented.

Methods and materials A new scanner is based on LYSO crystals coupled with SiPM, and it consists of 14 compact modules with a transaxial FOV of 180 mm in diameter. In this study, initial GATE simulation studies were performed to predict the spatial resolution, absolute sensitivity, noise equivalent count rate (NECR) and scatter fraction (SF) of the new design. Spatial wobbling acquisitions were also implemented. Finally, the obtained projections were reconstructed using analytical and iterative algorithms.

Results The simulation results indicate that absolute sensitivity is 1.42% which is appropriate than other commercial breast PET systems. The calculated SF and NECR in our design are 20.6% and 21.8 kcps. The initial simulation results demonstrate the potential of this design for breast cancer detection. A small wobble motion to improve spatial resolution and contrast.

Conclusion The performance of the dedicated breast PET scanner is considered to be reasonable enough to support its use in breast cancer imaging.

Keywords Dedicated breast PET · Monte Carlo simulation · NEMA · Wobbling

Introduction

Breast cancer is one of the leading causes of cancer death among women worldwide in the last century [1, 2]. Noninvasive imaging techniques such as ultrasound [3] and MRI [4] have been widely used in the detection of breast cancer [4, 5]. However, these conventional techniques are imperfect modality and have been faulted for its false-positive rate, limited specificity, sensitivity, and unnecessary surgical biopsies, especially in women [6]. A strategy for reducing

✉ Hossein Ghadiri
h-ghadiri@sina.tums.ac.ir

✉ Pardis Ghafarian
pardis.ghafarian@sbmu.ac.ir

✉ Parham Geramifar
pgeramifar@gmail.com

✉ Mohammad Reza Ay
mohammadreza_ay@sina.tums.ac.ir
http://www.mohammadreza-ay.net

[1] Research Center for Molecular and Cellular Imaging, Tehran University of Medical Sciences, Tehran, Iran

[2] Department of Medical Physics and Biomedical Engineering, Faculty of Medicine, Tehran University of Medical Sciences, Sina Campus, Tehran 1417613151, Iran

[3] International Campus, Tehran University of Medical Sciences, Tehran, Iran

[4] Chronic Respiratory Diseases Research Center, National Research Institute of Tuberculosis and Lung Diseases (NRITLD), Shahid Beheshti University of Medical Sciences, Tehran, Iran

[5] PET/CT and Cyclotron Center, Masih Daneshvari Hospital, Shahid Beheshti University of Medical Sciences, Tehran, Iran

[6] Research Center for Nuclear Medicine, Shariati Hospital, Tehran University of Medical Sciences, Tehran, Iran

Published online: 06 April 2020

breast cancer mortality is early detection for successful treatment. Positron emission tomography (PET) [7, 8] has proven to have better specificity and sensitivity in detecting tumor lesions than ultrasound and X-ray mammography [9]. PET is a useful technique to visualize biologic processes and molecular features within the body. It has the potential for improvement in the detection and diagnosis of cancers, problem-solving, treatment monitoring, and the identification and quantification of the specific biologic targets used to tailor therapy. PET with 18F-FDG has shown the potential to detect the disease early due to predicting poor outcome. The main advantage of metabolic imaging over conventional imaging is its ability to assess response earlier because the tumor metabolic changes occur before the morphologic changes [10].

Whole-body PET scanners do not appear to have adequate resolution for the detection of small lesions in the breast. Whole-body PET is not effective for local staging of the breast because their efficiency declines in detecting small lesions [11]. Except for the staging of metastatic disease beyond the breast, PET imaging is not routinely utilized in the evaluation of primary breast cancer. PET has proven to have better sensitivity and specificity in detecting tumor lesions than X-ray mammography. Dedicated PETs are based on high-resolution detectors placed close to the breast. This was the motivation for the development of them.

The dedicated PET systems are intended to have higher photon sensitivity and improved spatial resolution using smaller detector elements and bringing the detectors close to the breast. Dedicated breast PET scanners have been developed for the detection of subcentimeter-sized breast tumors. They are mainly classified into two groups. The first one can provide high spatial resolution by mildly compressing the breast with two parallel detectors [12] and the second scanner group acquires fully tomographic images of the breast [13]. Full-ring PET permits to circumvent such a limitation and can be used in assessing therapy response, staging and restaging of breast cancer. This was the motivation for the development of dedicated breast PETs.

The PEM/PET system developed at West Virginia University is a dual-head dedicated breast PET system [16]. Two sets of rotating planar detector (LYSO) heads acquire 3D imaging data and allow the composition of fully tomographic images. The biopsy capability is included in the system [14]. A dedicated breast PET/CT developed in University California Davis is a fully tomographic PET system with two PET detectors (LSO), a CT detector, and an X-ray tube that rotate in the coronal plane around a hanging breast of a patient lying in prone position [15]. Then, they used a new detector that holds DOI measurement capability and has a high intrinsic spatial resolution, which is expected to improve the spatial resolution of this system [16]. The MAMMI is a fully tomographic dedicated PET system with a complete ring shape detector, consisting of 12 identical detector modules that have a transaxial FOV of 170 mm in diameter, and a 40-mm-long axial FOV. MAMMI first got certification in Europe and recently gained the approval of the FDA in the United States in 2014 [17]. Elmammo (Shimadzu Co., Kyoto, Japan) is another type of a fully tomographic dedicated PET system with a complete ring-shaped detector (LGSO). The system consists of 36 detector blocks arranged in 3 contiguous rings with 12 detector modules, with a transaxial diameter of 185 mm and an axial FOV of 155.5 mm [18]. Conventional PET systems have detectors arranged in a ring to surround the object. Various methods can improve image resolution of scanners with a small diameter. For example, wobbling the PET system or the bed can also increase the spatial sampling in PET systems [19, 20]. The principle of the wobbling is to form a randomly overlapped datum that can be interpolated for fine high-resolution data to fulfill the Nyquist. By increasing wobbling number or wobbling stop points, in principle, infinitely high sampling is possible [21]. In this study, we have designed a dedicated high-resolution breast PET scanner based on the MR compatible detector modules, which we have already developed using LYSO crystal and SiPM photon sensors [22]. The main motivation behind this work is geometrical optimization and estimation of system performance using Monte Carlo simulation. Also, implementing the wobble motion mechanism may represent a cost-effective method to upgrade the contrast and spatial resolution.

Materials and methods

The designed dedicated breast PET (EstatiraPET) has four detector rings with an axial field of view (FOV) of 50 mm that translates; however, full imaging of breasts can require several acquisitions in step and shoot mode. An ideal system should have high sensitivity and the low cost. However, these requirements are often in conflict with each other.

Estatira PET is a dedicated high-resolution breast PET developed in which the acquisition is performed in the prone position and does not require compression of the breast such as conventional mammography and the direction of the acquisition is from the chest wall to the nipple. It uses scintillation crystals coupled to Silicon Photomultipliers (SiPMs). The detector ring consists of 14 detector modules (LYSO crystal) with a scanner aperture of 230 mm. The number of detectors depends on breast size. In this work, we have evaluated the performance of the 14-detector configuration of the EstatiraPET based on the measurements and procedures described for large breasts.

In this work, we have evaluated the performance of the 14-detector dedicated breast PET based on the measurements and procedures described in NEMA NU 4-2008

protocols [23]. The performance of the new system has been compared with that of the MAMMI dedicated breast PET [17]. Our goal in this work is to optimize the geometry breast scanner design by performing studies for estimating image uniformity and lesion activity uptake. This is the detector design that allows the operation of digital SiPMs simultaneously inside an MRI system. The operation of the digital SiPM is expected to be unaffected by strong magnetic fields and its intrinsic digitization should make it less prone to electromagnetic interference. So it optimized to be the MRI-compatibility and reduces distortions of the static magnetic field compared to a conventional design. Also, it has more transaxial FOV with adequate sensitivity and spatial resolution.

Each test requires that the operating parameters of the scanner be adjusted, as they would be for a typical patient study, including the energy window, axial acceptance angle, coincidence time window, and slice thickness. The data processing and reconstruction algorithms should also be the same as those used for a typical patient study, with the exception that some tests require the use of filtered back projection with a ramp reconstruction filter for standardization among systems. For all studies, complete angular sampling is acquired.

Description of the proposed block and the detector unit

Detector head consists of a scintillator array coupled to an SiPM device placed in an aluminum housing. We used SensL ARRAYC-30035-144P which is a 12×12 array of C-series SiPM technology pixels (SensL DS 2014). The active area of each SiPM is 3×3 mm^2 with 4.2 mm pixel pitch. In the current version of our generic detector block, we coupled the SiPM array to a 24×24 array of cerium-doped lutetium–yttrium oxyorthosilicate (LYSO:Ce) crystal with $2 \times 2 \times 10$ mm^3 pixels and 0.1-mm-thick barium sulfate ($BaSO_4$) inter-pixel reflector [22].

After detector designing, the proposed dedicated breast PET (EstatiraPET) is configured. The system has an axial field of view (FOV) of 50 mm that translates; however, full imaging of breasts can require several acquisitions in step and shoot mode.

Simulated breast PET description

The system consists of 14 detector blocks arranged in 24 contiguous rings, with a ring diameter of 230 mm and an axial FOV is 50 mm. Each detector block is composed of a 24×24 array of LYSO crystals coupled to SiPMs. Each crystal is 10 mm long and has a cross-sectional area of 2×2 mm. Barium sulfate (or sulphate) with the chemical formula $BaSO_4$ with 0.1 mm length which is used as the insertion of the inner crystal reflector between crystal elements to control the behavior of scintillation photons. The detector can record incidence within an energy window of 350–650 keV and the coincidence window of 5 ns is applied to the acquired data. The transaxial FOV has a diameter of about 190 mm and the axial FOV is 50 mm. The system could acquire data in 3D mode.

The Monte Carlo simulation model of dedicated breast PET

GATE version 7.2 which is open-source code is used to model the Monte Carlo simulation of the breast PET system. GATE incorporates the GEANT4 libraries and combines the GEANT4's strength of precise geometry modeling tools, well-validated physic process model and efficient visualization [24]. The cylindrical EstatiraPET GATE model has been developed by the description below. In this work, the main photon physics processes were simulated, including photoelectric effect, Compton and Rayleigh scattering. All simulated experiments had a coincidence timing window of 5 ns and a 511 keV; photopeak energy resolution of 20%. The application of GATE allows modeling various components of the PET system, including system geometry configuration, physic process, source selection, and signal-processing chain. The performance of the EstatiraPET was evaluated at energy windows: 350–650 keV. A modeled view of the breast PET scanner is shown in Fig. 1. The simulation measurements were done and compared the results with MAMMI breast PETs with a different design. The phantoms, sources, and measurements proposed in NEMA standards [23] were conveniently adapted to evaluate the performance of the scanner since the characteristics of dedicated breast PETs do not exactly suit none of them. In our simulation, photoelectric effect, Compton, Rayleigh, and multiple scattering, pair production, ionization, non-collinearity, positron range, and radioactive decay are considered.

We applied 5 ns FWHM time resolution, which is similar to reported values when using similar detector configurations. We used ROOT and ASCII output to analyze the results.

Geometry optimization

The design of instrumentation for PET scanners has vastly progressed over the past 10 years. A primary challenge of a dedicated breast scanner is having high sensitivity and spatial resolution, and also the low cost of the scanner. In three systems, rings consist of 10, 12 and 14 LYSO modules, with scanner aperture of 162 mm, 196 mm and 230 mm. The new designs combine high spatial resolution and high sensitivity to detect small and low-contrast masses.

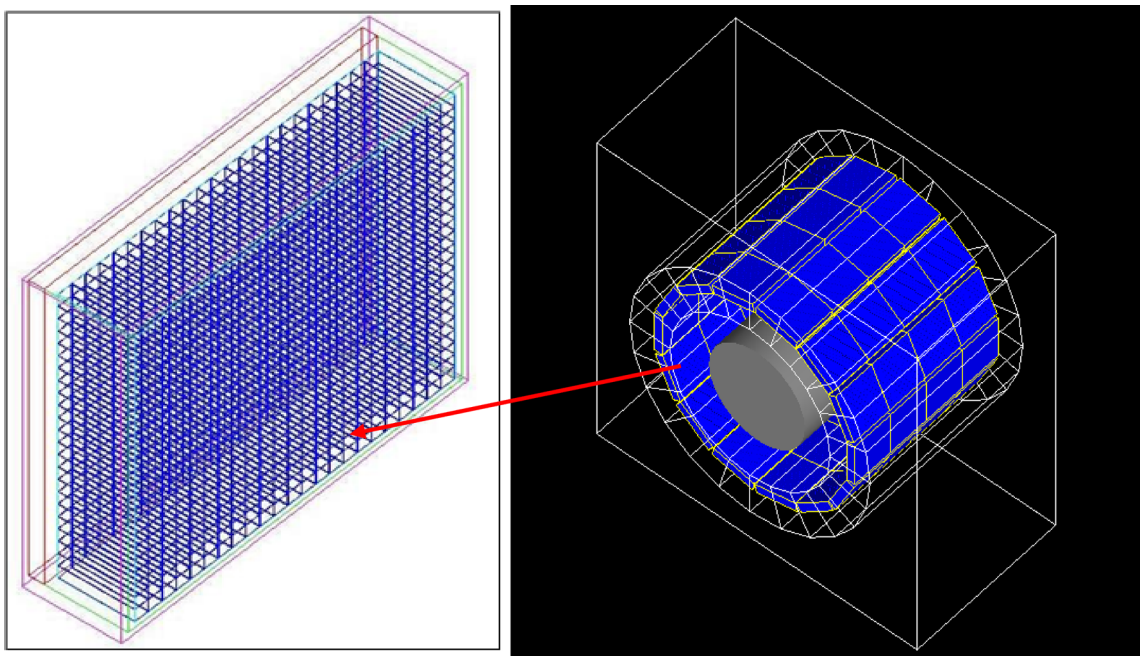

Fig. 1 Geometry architecture of the EstatiraPET system modeled in GATE. Besides, an expanded view of the detector module, block, and crystal arrangement is shown

Validation study

Model verification: We verified the correctness of the EstatiraPET model by plotting the coordinates of the detected photons in both the axial and the transaxial directions as a response to a point source at the FOV center similar to [25]. We performed several simulations to validate the EstatiraPET scanner model: MAMMI scanner simulation, point-source sensitivity, noise equivalent count rate (NECR), and scatter fraction (SF). The results were evaluated and compared with the experimental MAMMI's data, as well as those reported in the literature [26].

Sensitivity Aiming to ensure the accuracy of the simulation model, this efficiency factor was determined until a reasonable agreement with NEMA experimental measurement. An energy threshold of 350 keV and a 5-ns coincidence window were selected for this simulation. A 10 μCi (0.37 MBq) 18F spherical point source of diameter 2 mm was placed inside a plastic sphere, 1 mm in diameter at the center of the FOV that was moved along the axis of the scanner in step sizes of 1.07 mm (slice thickness) and data were acquired for 1 s.

Noise equivalent counts (NECR) and scatter fraction (SF) NECR and SF of this design were evaluated with a cylindrical phantom containing a line source insert. A phantom composed of breast tissue was simulated and placed at the center of the scanner. It had a diameter of 80 mm and a length of 50 mm. A 1 mm diameter line source was 50 mm long and NECR was calculated for different activity values. NECR and SF were defined in the following equations, where T, S, and R are true, scatter and random coincidence rate, respectively. $K=1$ was used to denote a noiseless random correction.

$$\mathrm{NECR} = \frac{T^2}{(T+S+KR)} \tag{1}$$

$$\mathrm{SF} = \frac{S}{(T+S+R)}. \tag{2}$$

Spatial resolution A point source consisting of a sphere of Na-22, radius 0.25 mm, and surrounded by a 10-mm-thick plastic wall. The source activity and acquisition time were 10 μCi (0.37 MBq) and 1 s, respectively. Point source sensitivity is defined as the fraction of 511 keV true coincidence photon events detected for a point source with a given activity placed in the center of FOV that was positioned at radial distances 5 to 80 mm away from the center of the system. Images were reconstructed using the 3D filtered back projection using STIR (Software for Tomographic Image Reconstruction) package.

Image analysis After performing a sensitivity analysis, we evaluated the reconstructed spatial resolution of the EstatiraPET. The point source was placed with a radial step of 1 mm in X and Y directions. The reconstructions were performed

with a three-dimensional filtered back projection (FBP) and iterative ordered subset expectation maximization (OSEM) method (15 iterations). To perform a detailed qualitative evaluation, a point source in the center of the scanner was simulated and then reconstructed using the OSEM algorithm. Aimed at spatial resolution calculation, the reconstructed images of point source arrays were measured by fitting a Gaussian function to the plotted profiles, thus calculating their FWHM. For spatial resolution calculations, the reconstructed images of point source arrays were measured by fitting a Gaussian function to the plotted profiles and thus calculating their FWHM. To assess the reconstructed image quality of full ring EstatiraPET, the Derenzo phantom was simulated. The Derenzo phantom was modeled with spheres of different diameters (1, 1.25, 1.5, 2, and 2.5 mm) with the activity of 5, 6, 7.5, 10, and 12.5 MBq comprising back-to-back gamma sources, arranged into five segments. All data were reconstructed using 3D-FBP and 3D-OSEM (10 iterations) using the STIR reconstruction framework [17] and then the images were obtained. To illustrate the resolution resolving as contrast criteria, the intensity of line profiles crossing the spheres in the Derenzo phantom was plotted.

Proof of the new geometry design concerning the real PET scanner To validate the application of GATE (Geant4 Application for Tomographic Emission) Monte Carlo simulation toolkit and a simulated new scanner, we modeled a realistic PET (MAMMI PET) system that is designed with cylindrical geometry and block detectors. The scanner is made by 10 LYSO modules in a ring with a 162 mm diameter. SiPM is used for optical detection. We compared our simulation with the measurement made on the scanner that was evaluated. For validation of our simulation, we compared the simulated spatial resolution of the point source. This parameter was measured by the full-width half-maximum (FWHM) which is the width of the point spread profile at half of its maximum. This validation process allowed us to validate the accuracy of our simulation code and also the algorithm developed to reconstruct the image. The specifications of the simulated PET (EstatiraPET) and MAMMI scanners are presented in Table 1.

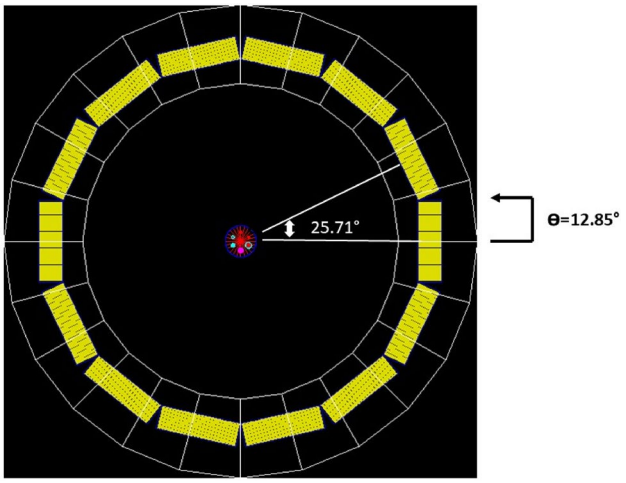

Fig. 2 Wobbling radius is about half a block detector size to cover the gaps

To perform spatial resolution and sensitivity comparisons, a 1 MBq back-to-back gamma point source was placed in the center of transaxial FOV in ideal conditions.

Wobble radius for EstatiraPET To reconstruct image resolution and artifact reduction from increased sampling, but without improving LOR resolution, the wobbling technique was assessed. The principle of the wobbling technique is to form a randomly overlapped linear datum each of which are sparsely sampled, that wobbled sampling is related to half of the crystal pitch. To determine the optimal wobble radius for the EstatiraPET scanner, the overall shape and FWHM of profiles in the sinograms from a simulation of scanning of a ^{22}Na point source with activity 1 μCi were compared. In this work, the highlighted improvement in spatial resolution for the EstatiraPET was obtained in different wobble radius (Fig. 2).

Table 1 Specifications of the simulated PET (EstatiraPET) and MAMMI scanners

Specification	EstatiraPET (14 module)	MAMMI PET (12 module)
Ring diameter (mm)	230	186
Crystal size (mm)	$2\times2\times10$ mm^3	–
Number of crystals per block (module)	24×24 (576)	Monolithic
Number of the transaxial blocks (module)	14	12
Material	LYSO	LYSO
Number of rings	24×4	4
Axial FOV (mm)	50 mm	40 mm
Transaxial FOV (mm)	~ 190	170

Results

Geometry design

The detector ring consists of 14 detector modules (LYSO crystal) with a scanner aperture of 230 mm, 12 detector modules (LYSO) with a scanner aperture of 196 mm and the crystal thickness is of 10 mm. The number of detectors depends on breast size. In patients with large breasts 14 detectors, whereas in patients with smaller breasts only 12 rings, are acquired. In this work, we have evaluated the performance of the 14-detector configuration of the EstatiraPET based on the suitable FOV for large breasts. The results obtained indicate that the FOV in three different ring sizes, for 10, 12, and 14 detectors for cylindrical new PET geometry, is 120 mm, 149 mm, and 180 mm in sequence (Fig. 3). As shown in Fig. 3b, the primary impact of increasing ring diameter is to decrease the sensitivity of the scanner. Therefore, we use 14 detectors for dedicated breast PET. The direction of the acquisition is from the chest wall to the nipple. The number of ring positions depends on breast size. In patients with large breasts, 3 or 4 ring positions are used. In this work, we have evaluated the performance of the 14-detector and four-ring configuration of the EstatiraPET based on the measurements and procedures described for more than 70% of breast size in transaxial diameter.

Sensitivity

The sensitivities of the cylindrical LYSO system with a different number and detector modules and ring diameters (transaxial FOV) are summarized in Table 2. It should be noted that we can improve the geometrical sensitivity by increasing parameter axial FOV or decreasing the ring diameter of the scanner. The sensitivity will be decreased to 230 mm FOV but we used this configuration to be able to cover all breast sizes during the imaging. Our results indicate that a scanner based on any of the 14-detector design

Table 2 Sensitivity results based on #modules and ring diameter

Ring diameter (mm)	Number of modules	Sensitivity (cps/kBq)
230	14	13.8
196	12	15
162	10	15.25

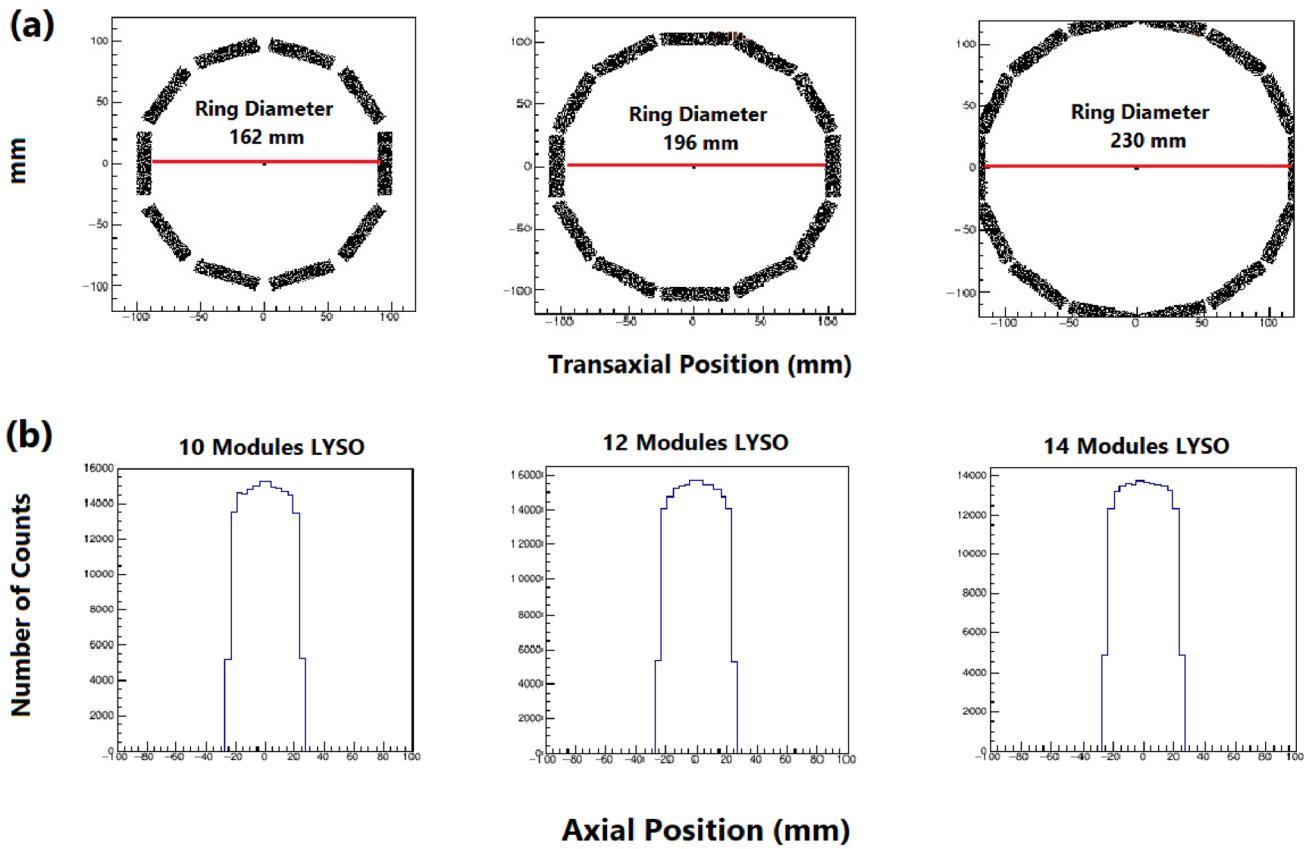

Fig. 3 **a** Transaxial and **b** axial detection position in simulation results in different geometry

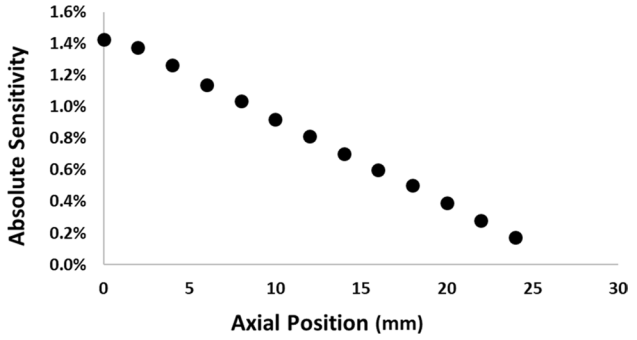

Fig. 4 Axial absolute sensitivity profile along the *z*-axis of Estatira-PET (14 detector modules) camera

Table 3 Comparison of scatter fraction (%) NECR peak (KCPS @ MBq) measured in two energy windows

Energy (keV)	350–650	250–750
SF (%)	20.6	20.8
NECR	21.8	25

would offer adequate sensitivity and uniform spatial resolution needs to scan.

The system peak absolute sensitivity was 1.42% at the center of the axial and transaxial FOVs. The axial sensitivity profile obtained by plotting the absolute sensitivity for each slice number is shown in Fig. 4.

NECR and SF

The SF and NECR for the line source in breast tissue were simulated at two energy windows around 511 keV as shown in Table 3. The scatter fraction for an energy window of 250–750 keV is 20.8 and for a narrower energy window of 350–750 keV, this value is reduced to 20.6. The highest NECR was achieved in the energy window of 250–750 keV. The two energy windows had comparable NECR.

Spatial resolution

The customary procedure for obtaining the spatial resolution is to measure the width of the point spread function (PSF) of the reconstructed point source on the image. The spatial resolution for the point source was simulated at the energy window of 350–650 keV. The spatial resolution degrades as the point source is moved away from the axis of the scanner. The spatial resolutions of FWHM at different positions are reported in Figs. 5, 6, and 7. The radial component was especially affected by the transaxial displacement.

The measurement of the spatial resolution of a point-like source is compared with experimental data in three

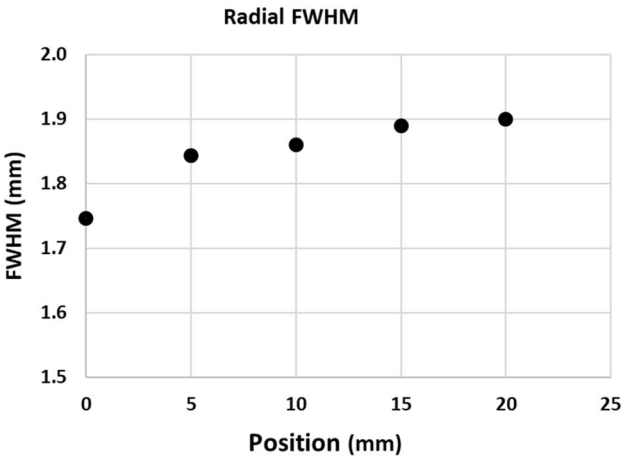

Fig. 5 The spatial resolution values for point source array in the radial direction in center of FOV

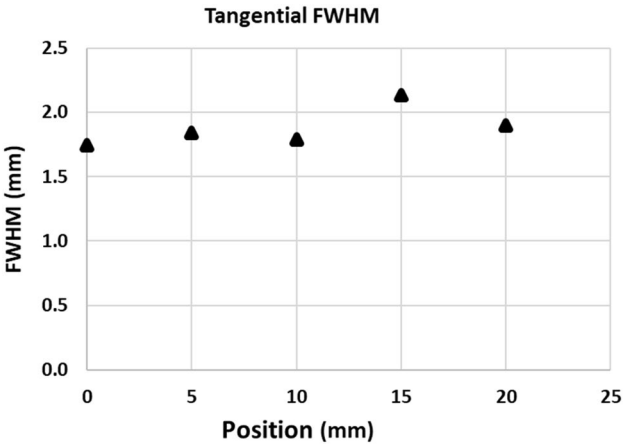

Fig. 6 The spatial resolution values for a point source in the tangential direction in center of FOV

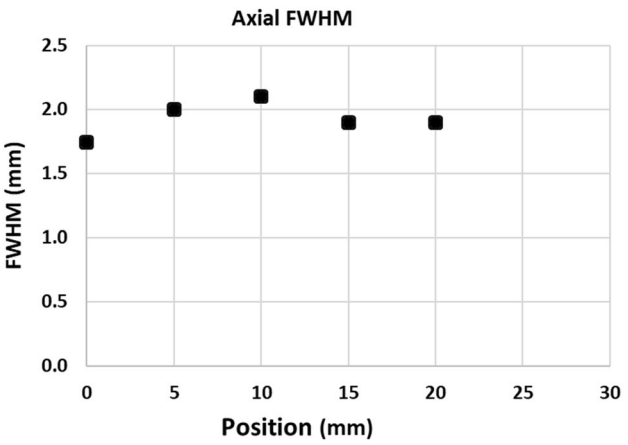

Fig. 7 The spatial resolution values for point source array in the axial direction in center of FOV

directions. The FWHM for all positions can reach between 1.7 and 2 mm.

Image analysis

Figure 8 shows the sinograms and reconstructed images of the phantom with point source arrays, providing the basis for a spatial resolution analysis of the full-ring scanner using FBP and OSEM algorithms. In Fig. 8c, we show the central slice of the reconstructed image using OSEM. We observe that the blurring is reduced when we use the iterative reconstruction algorithm, although the images of the spherical sources are relatively stretched in the EstatiraPET scanner with the FBP method (Fig. 8b).

Optimum wobble radius

The average of the FWHMs is calculated from the FWHMs from ten different positions on sinograms for each wobble radius. When the wobbling motion is set to be 12.75°, the source profiles do not have the minimum FWHMs. This value is slightly smaller than half of the crystal pitch used in the EstatiraPET scanner. The improvement from only more sampling from angular wobbling is outstandingly good compared to the stationary mode in image quality in the Derenzo phantom (Fig. 9). It shows a slice of the transverse image of the phantom and its profile with and without the wobble effect. The upper profile (a) and image (b) are shown for the stationary mode and the bottom profile (c) and image (d) are for the wobbled scan. Without wobble motion, rod diameters of 2.5 and 3 mm in the phantom are hardly distinguishable in the image (b). In comparison, most rods of diameter 2.5 mm can be recognized in the wobbled image (d) of Fig. 9. The profiles (a) and (c) were generated from the selected area on the images (b) and (d), respectively.

The comparison of the performance of an EstatiraPET and MAMMI scanners with GATE simulation is shown in Table 4.

Discussion

In this study, we investigated the performance of a cylindrical dedicated breast PET with GATE simulation. To this aim, the GATE platform was used to model the scanner configuration and relevant physical process. Functional imaging with PET using FDG has an advantage over anatomical imaging in that it relies on the differences in metabolic activity between normal and abnormal tissues. We modeled the performance characteristics according to NEMA NU-2 2008 standards and the results were validated focusing on system resolution, sensitivity, counting rates and NECR. The developed model is accurate enough to be applied in a wide range of applications and it is beneficial for system development. It enables us to evaluate the system performance under various acquisition conditions and can be used to obtain information that is difficult to be measured in the practical experiment, such as scatter, system point spread function in PET imaging.

In this study, we investigated the performance of an EstatiraPET scanner with GATE simulation. The EstatiraPET has an axial FOV of 48.3 mm with high sensitivity and allows making possible with a lower dose scanning. The improvement in sensitivity in EstatiraPET leads to a substantial increase in the number of counts registered at a given activity, sensitivity is 1.42% which is comparable to other commercial PET systems such as 1.8% of the MAMMI PET [17]. Spatial resolution values below 2 mm were measured in most of the FOV (in axial, tangential, and radial). The spatial resolution measured at the center of the axial FOV of EstatiraPET is better than that measured in the MAMMI scanner. The effective field of view has a diameter of 180 mm in our

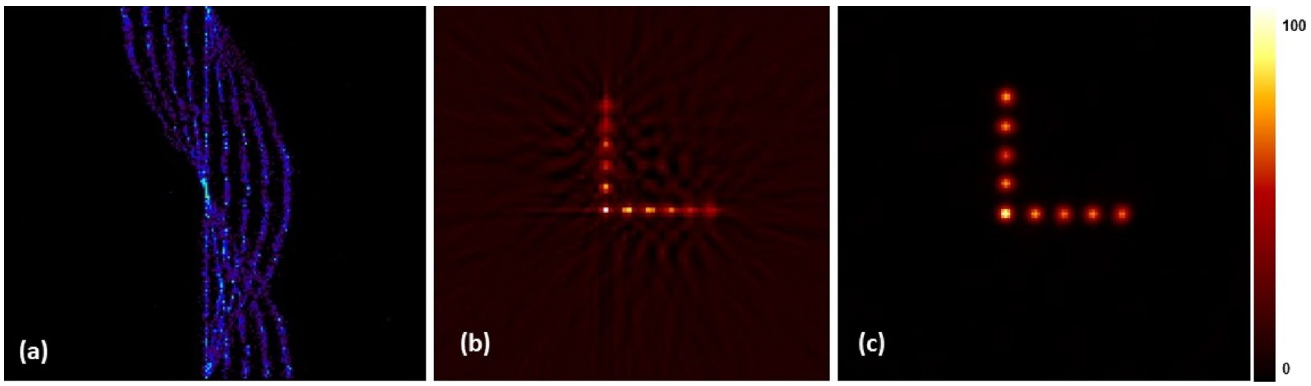

Fig. 8 The sinogram of point source array EstatiraPET scanner (**a**). The reconstructed image of a point source array by FBP (**b**). The reconstructed image of a point source array by OSEM (**c**)

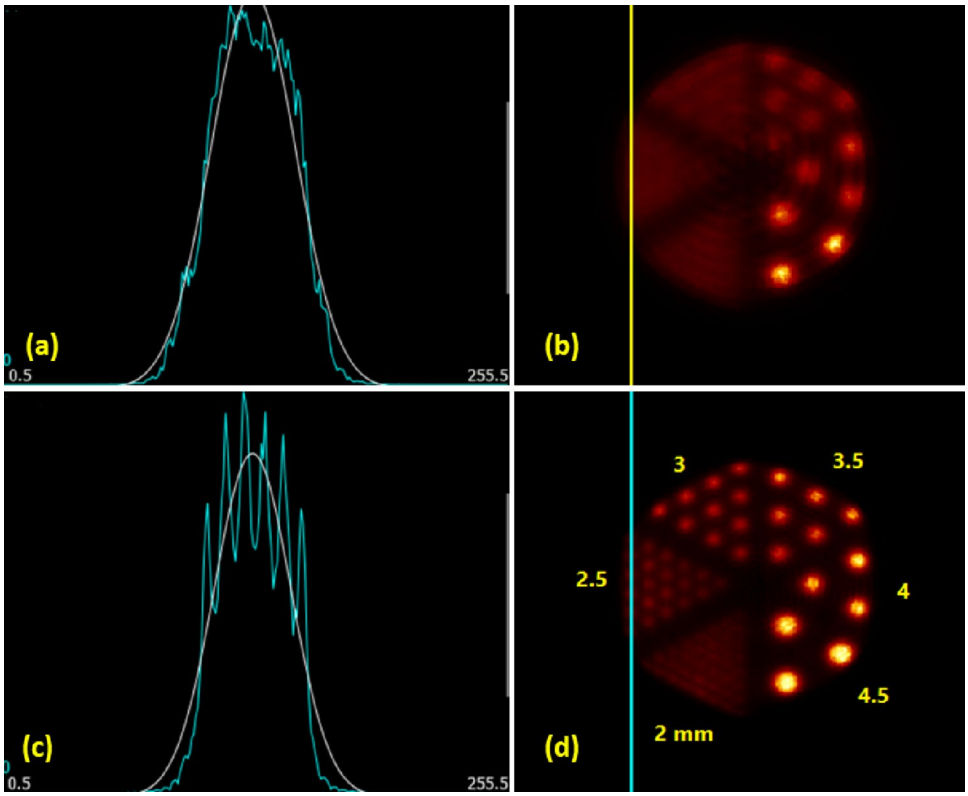

Fig. 9 The upper profile (**a**) and image (**b**) correspond to data acquired without wobble motion. The bottom profile (**c**) and the image (**d**) are from the data acquired with wobble motion

Table 4 Comparison of performance of an EstatiraPET and MAMMI scanners with GATE simulation

Parameter	EstatiraPET	MAMMI PET
AFOV	50 mm	40 mm
Transaxial FOV	~ 190 mm	170 mm
Crystal	LYSO	LYSO
Spatial resolution	1.7–2 mm	1.6–2 mm
Absolute sensitivity	1.42%	1.8%
# Detector module (per ring)	14	12

scanner; however, it is 170 mm in MAMMI. The developed detector ring is compatible with the MRI system because Si-PM is insensitive to the static magnetic field.

In this work, the highlighted improvement in spatial resolution for the EstatiraPET was obtained when a wobble radius slightly smaller than half of the crystal pitch was used. If the wobble radius is larger than crystal pitch, a larger overlapping area between two adjacent detectors may make the relative concentration of data in adjacent bins unacceptably large. Visual inspection of the micro-Derenzo phantom images showed that the wobbling mechanism improved the spatial resolution of EstatiraPET scanner. The image from the wobbled scan shows improved contrast when compared to the stationary mode. Also, the improvement of the spatial resolution of images is cleared. Although the computational simulation makes limitations but it enables us to evaluate the system performance under various acquisition conditions and can be used to obtain information that is difficult to be measured in the practical experiment. The initial simulation results demonstrate the capability of this PET system for breast cancer detection. In the future study, we will use the partial geometry model (some detector blocks turned off) for including some advantages such as reducing the cost of the scanner to make it more accessible to users, scan time and MRI compatible. We will use new compressive sensing (CS) techniques in breast PET imaging to investigate the feasibility of decreasing the number of detectors while maintaining image quality.

Conclusion

We have presented a simple yet realistic Monte Carlo code for PET imaging simulation based on GATE. This model had been validated against the experimental results obtained from the real measurement. The comparison shows that the spatial resolutions and sensitivity of the simulated and measured images are in a good agreement. Thus, this study proves that our GATE code of PET scanner and also all the post-simulated programs can reproduce the condition of the real PET scanner imaging. We have designed a dedicated breast PET based on pixelated LYSO crystals. Its performance has

been fully assessed using NEMA NU 4-2008 adapted protocols. When compared with other dedicated breast PET scanners, MAMMI exhibits similar performance characteristics, and in many cases, it is better than that is more complex and expensive. A low-cost technique can be added to the PET scanner to improve its spatial-resolution with wobbling. Our detector ring is compact and the outer diameter of the ring is small; developed detector ring can easily be set in narrow space of the MRI gantry.

Further improvements are foreseen shortly for the PET scanner that we have presented in this work. These improvements consist of a PET equipped with the partial ring which is currently being developed. With these modifications, MAMMI sensitivity and counting rate capabilities will increase significantly. However, the values remain comparable to other dedicated breast PETs, and to sum up, EstatiraPET is suitable to be used in breast scanning and cancer detection.

References

1. Rajaraman P, Anderson BO, Basu P, Belinson JL, D'Cruz A, Dhillon PK, et al. Recommendations for screening and early detection of common cancers in India. Lancet Oncol. 2015;16(7):e352–e361361.
2. Stewart B, Wild CP. World cancer report 2014. Health. 2017.
3. Berg WA, Bandos AI, Mendelson EB, Lehrer D, Jong RA, Pisano ED. Ultrasound as the primary screening test for breast cancer: analysis from ACRIN 6666. JNCI J Natl Cancer Inst. 2016;108(4):djv367.
4. Lehman CD, Lee JM, DeMartini WB, Hippe DS, Rendi MH, Kalish G, et al. Screening MRI in women with a personal history of breast cancer. J Natl Cancer Inst. 2016;108(3):djv349.
5. Peters NH, Borel Rinkes IH, Zuithoff NP, Mali WP, Moons KG, Peeters PH. Meta-analysis of MR imaging in the diagnosis of breast lesions. Radiology. 2008;246(1):116–24.
6. Haas BM, Kalra V, Geisel J, Raghu M, Durand M, Philpotts LE. Comparison of tomosynthesis plus digital mammography and digital mammography alone for breast cancer screening. Radiology. 2013;269(3):694–700.
7. Granov A, Tiutin L, Schwarz T. Positron emission tomography. Berlin: Springer Science & Business Media; 2013.
8. Madsen M. Quantitative analysis in nuclear medicine imaging. Med Phys. 2007;34(4):1522.
9. Fowler AM. A molecular approach to breast imaging. J Nucl Med. 2014;55(2):177–80.
10. Groheux D, Espié M, Giacchetti S, Hindié E. Performance of FDG PET/CT in the clinical management of breast cancer. Radiology. 2013;266(2):388–405.
11. Thompson C, Murthy K, Weinberg I, Mako F. Feasibility study for positron emission mammography. Med Phys. 1994;21(4):529–38.
12. Belcari N, Guerra A. High-resolution and animal imaging instrumentation and techniques. Handbook of particle detection and imaging. Berlin: Springer; 2012. p. 1125–1151.
13. MacDonald L, Edwards J, Lewellen T, Haseley D, Rogers J, Kinahan P. Clinical imaging characteristics of the positron emission mammography camera: PEM Flex Solo II. J Nucl Med. 2009;50(10):1666–755.
14. Raylman RR, Majewski S, Smith MF, Proffitt J, Hammond W, Srinivasan A, et al. The positron emission mammography/tomography breast imaging and biopsy system (PEM/PET): design, construction and phantom-based measurements. Phys Med Biol. 2008;53(3):637.
15. Bowen SL, Wu Y, Chaudhari AJ, Fu L, Packard NJ, Burkett GW, et al. Initial characterization of a dedicated breast PET/CT scanner during human imaging. J Nucl Med Off Publ Soc Nucl Med. 2009;50(9):1401.
16. Godinez F, Chaudhari AJ, Yang Y, Farrell R, Badawi RD. Characterization of a high-resolution hybrid DOI detector for a dedicated breast PET/CT scanner. Phys Med Biol. 2012;57(11):3435.
17. Moliner L, Gonzalez A, Soriano A, Sánchez F, Correcher C, Orero A, et al. Design and evaluation of the MAMMI dedicated breast PET. Med Phys. 2012;39(9):5393–404.
18. Miyake KK, Matsumoto K, Inoue M, Nakamoto Y, Kanao S, Oishi T, et al. Performance evaluation of a new dedicated breast PET scanner using NEMA NU4-2008 standards. J Nucl Med. 2014;55(7):1198–203.
19. Brooks RA, Sank VJ, Di GC, Friauf WS, Leighton SB. Design of a high resolution positron emission tomograph: the Neuro-PET. J Comput Assist Tomogr. 1980;4(1):5–13.
20. Bohm C, Eriksson L, Bergstrom M, Litton J, Sundman R, Singh M. A computer assisted ringdector positron camera system for reconstruction tomography of the brain. IEEE Trans Nucl Sci. 1978;25(1):624–37.
21. Cho Z-H, Son Y-D, Kim H-K, Kwon D-H, Joo Y-H, Ra JB, et al. Development of positron emission tomography with wobbling and zooming for high sensitivity and high-resolution molecular imaging. IEEE Trans Med Imaging. 2019;38(12):2875–82.
22. Salar S, Navid Z, Mohsen T, Sanaz K, Hadi K, Saeed S, et al. Generic high resolution PET detector block using 12 × 12 SiPM array. Biomed Phys Eng Express. 2018;4(3):035014.
23. Association N. NEMA Standards Publication NU 4-2008. Performance measurements of small animal positron emission tomographs. 2008.
24. Conti PS, Lilien DL, Hawley K, Keppler J, Grafton ST, Bading JR. PET and [18 F]-FDG in oncology: a clinical update. Nucl Med Biol. 1996;23(6):717–35.
25. Geramifar P, Ay M, Zafarghandi MS, Sarkar S, Loudos G, Rahmim A. Investigation of time-of-flight benefits in an LYSO-based PET/CT scanner: a Monte Carlo study using GATE. Nucl Instrum Methods Phys Res Sect A. 2011;641(1):121–7.
26. Moliner L, Gonzalez A, Soriano A, Sanchez F, Correcher C, Orero A, et al. Design and evaluation of the MAMMI dedicated breast PET. Med Phys. 2012;39(9):5393–404.